SOLUTION OF INTERNAL LAMINAR FLOWS THROUGH CFD: MULTIGRID METHOD FOR CONVERGENCE ACCELERATION

José Antonio Rabi
Faculdade de Engenharia Civil – PUC Minas / Poços de Caldas
Av. Pe. Francis Cletus Cox, 1661, Jd. Country Club, Poços de Caldas, 37701-355, MG, Brazil
tel: +55 35 3697-3000, fax: +55 35 3697-3001, e-mail:jrabi@pucpcaldas.br

ABSTRACT

Air flow modeling and simulation are important for HVAC&R design and optimization. Nevertheless, if detailed and accurate information is desired, fine meshes should be used, which tends to increase the computational effort. Multigrid methods are known to reduce such effort and a preliminary V-cycle correction-storage multigrid program is under development in order to numerically solve steady-state two-dimensional laminar flows. Structured, orthogonal and irregular meshes are employed following a finite-volume discretization. As a first trial, a given simple laminar flow problem was considered. The corresponding flow pattern is qualitatively checked out and residue reduction histories are presented.

1. INTRODUCTION

Numerical methods have been used to solve fluid mechanics and heat transfer problems and solutions so obtained have proved to be reliable, even in rather complex instances. Computational Fluid Dynamics (CFD) programs have been extensively developed thanks to low cost, large memory capacity and fast computers in conjunction with efficient and precise numerical methodologies (MALISKA, 1995).

Computational simulation is already incorporated to thermal comfort problems (BARROS et al., 2001; CUNHA et al., 2001; MÁXIMO and BERTE, 2001; MENDES and CELINSKI, 2001; MORAES and LABAKI, 2001; SCHMID, 2001). As far as ventilation is concerned, air velocity fields might be properly achieved by means of CFD (FERNÁNDEZ and EGUÍA, 2001; LÔBO and BITTENCOURT, 2001). Nevertheless, computing time should not be prohibitive if high accuracy is a desired feature.

Accordingly, a CFD program has been developed in Fortran-90 so as to provide numerical solutions of internal flow problems. At its present stage, the CFD method employed finite-volume formulation, SIMPLE pressure-velocity coupling and multigrid convergence acceleration. This paper compares the CPU time (i.e. computational effort) needed by the program to solve a given steady-state laminar two-dimension flow employing different numbers of computational grids.

2. AIR FLOW MODELING AND SIMULATION

Modeling and simulation play an important role in design and optimization, particularly in those cases for which analytical do not apply or experimental methods are somewhat unfeasible. In principle, a comprehensive mathematical model and its corresponding computational program should cover important phenomena of the process. In view of that, design parameters should be confidently predicted and experimental data should be reproduced within acceptable levels of accuracy.

2.1 Space and Time Orders of a Mathematical Model

Depending on its degree of sophistication, output data provided by a simulation model may vary from a set of global parameters up to a detailed (point-to-point) description of physical quantities of interest (e.g. temperature, pressure, moisture content) within a three-dimensional transient flow field.

Zero-order models consider no space-dependent equations to evaluate internal processes. First-order models take into account one-dimension variations inside the process. Second-order models should be evoked when variations along another dimension cannot be neglected. Due to inherent complexities, third-order models are less often adopted, although a great deal of information about the process might be obtained if all space coordinates are successfully regarded.

If time variations are considered, the model is dynamic; otherwise it is based on a steady-state approach. Particularly in thermal comfort problems, a (24-hour) periodic regime may be adopted.

2.2 Transport Phenomena Equations

HVAC&R problems may be tackled as transport phenomena applications. Whereas air flow is governed by the continuity and Navier-Stokes equations, moisture transfer is modeled by Fick's law. Since heat transfers are usually present, the first law of thermodynamics should also be evoked. Despite such transport processes occur simultaneously, it is convenient to split them up for the sake of formulation and solution. As the corresponding differential equations are coupled, analytical solutions are rare (if not impossible!). Simplifying assumptions should be carefully introduced so as to prevent the problem from moving away from reality, jeopardizing the quality of the numerical solution.

Governing equations for mass, momentum and energy conservation principles may be put into a mutual form known as the general transport equation (GTE). If ϕ and t represent the intensive property being transported and time respectively, the GTE for a Cartesian coordinate system (x, y, z) is expressed as:

$$\frac{\partial}{\partial t}(\rho\phi)+\frac{\partial}{\partial x}(\rho v_x\phi)+\frac{\partial}{\partial y}(\rho v_y\phi)+\frac{\partial}{\partial z}(\rho v_z\phi)=\frac{\partial}{\partial x}\left(\Gamma_\phi\frac{\partial\phi}{\partial x}\right)+\frac{\partial}{\partial y}\left(\Gamma_\phi\frac{\partial\phi}{\partial y}\right)+\frac{\partial}{\partial z}\left(\Gamma_\phi\frac{\partial\phi}{\partial z}\right)+S_\phi \qquad (1)$$

where ρ is the fluid density, Γ_ϕ is the diffusion coefficient, S_ϕ includes non-diffusive source (or sink) terms and v_x, v_y and v_z are the Cartesian components of the velocity vector $\vec{v}$.

Conservation equations are obtained by suitably replacing ϕ, S_ϕ and Γ_ϕ in Eq. (1), a procedure that depends on the flow regime. Table 1 summarizes the substitutions for a typical two-dimension laminar incompressible Γ_ϕ-constant flow. It is worth remembering that all z-direction terms are dismissed.

Table 1. Terms to be replaced into the GTE for two-dimension laminar incompressible flows.

Conservation equation	ϕ	Γ_ϕ	S_ϕ
bulk mass	1	0	0
x-momentum	v_x	μ	$-\frac{\partial p}{\partial x}$
y-momentum	v_y	μ	$-\frac{\partial p}{\partial y}$
energy	T	λ / c_p	S_T
i-component mass	C_i	$\rho D_{i,M}$	S_i

In the momentum equations, μ is the fluid viscosity and S_ϕ includes the pressure gradient. In the energy equation, T is the temperature, Γ_ϕ relates the fluid thermal conductivity λ to its constant-pressure specific heat c_p and S_T retains external energy source or sink terms (e.g. solar radiation). For the *i*-component mass transport, C_i and $D_{i,M}$ are respectively its concentration and diffusivity within the mixture while S_i comprises external mass sinks or sources (e.g. chemical reactions).

Although the conservation principles apply to any sort of problem, they cannot alone describe distinctive physical behavior of a given material. For that reason state equations are required. From a mathematical viewpoint, that comes from the fact that the number of unknowns exceeds the number of equations. For a compressible flow, an additional state equation is needed, which could be of the kind:

$$\rho = \rho(p, T) \tag{2}$$

Hence, for the five unknowns ρ, v_x, v_y, p and T there should be five equations (mass, x and y momentum, energy and state). For turbulent flows, different definitions for ϕ, S_ϕ and Γ_ϕ are needed (MALISKA, 1995). Moreover, a turbulence model should be evoked as for instance the turbulent kinetic energy / dissipation model, also simply referred to as the k-ε model (WHITE, 1991).

3. NUMERICAL SOLUTION OF FLOW PROBLEMS

The choice among the various modeling orders should be based on necessity, since sophistication does not guarantee quality. Conversely, too much simplicity may lead to false hypothesis about the flow. Anyhow, a model has no use if it cannot reproduce experimental data. Numerical simulation of velocity flow fields is a complex task, even for steady-state regimes, disregarding moisture and heat transfers (last two lines in Table 1). If such conditions are met as a first approach, substitution of the first three lines of Table 1 in the GTE, Eq. (1), results in the following system of coupled differential equations:

$$\frac{\partial}{\partial x}(\rho v_x) + \frac{\partial}{\partial y}(\rho v_y) = 0 \tag{3}$$

$$\frac{\partial}{\partial x}(\rho v_x^2) + \frac{\partial}{\partial y}(\rho v_y v_x) = \frac{\partial}{\partial x}\left(\mu \frac{\partial v_x}{\partial x}\right) + \frac{\partial}{\partial y}\left(\mu \frac{\partial v_x}{\partial y}\right) - \frac{\partial p}{\partial x} \tag{4}$$

$$\frac{\partial}{\partial x}(\rho v_x v_y) + \frac{\partial}{\partial y}(\rho v_y^2) = \frac{\partial}{\partial x}\left(\mu \frac{\partial v_y}{\partial x}\right) + \frac{\partial}{\partial y}\left(\mu \frac{\partial v_y}{\partial y}\right) - \frac{\partial p}{\partial y} \tag{5}$$

3.1 Finite Volume Formulation

Since the CFD simulator is at an initial stage, the present work considered the two-dimension pilot flow geometry sketched in Fig. 1*a*. The corresponding boundary conditions are also shown. The finite-volume method divides the solution domain into a number of rectangular control volumes (CVs). Should these CVs have different sizes, the resulting mesh would be structured, orthogonal and non-uniform.

Following a cell-centered scheme, grid points occupy the CV geometric center, as sketched in Fig. 1*b*. Storing the numerical values for the velocity components v_x and v_y and for the pressure p at these points is what characterizes a collocated arrangement.

Algebraic equations were obtained after integrating Eqs. (3), (4) and (5) over the CV sketched in Fig. 1*b*. Noting that $\delta V = \delta x\, \delta y$ and based on the GTE, Eq. (1), such integration is generally expressed as:

$$\int_{\delta v}\left[\frac{\partial}{\partial x}(\rho v_x \phi)+\frac{\partial}{\partial y}(\rho v_y \phi)\right] dV = \int_{\delta v}\left[\frac{\partial}{\partial x}\left(\Gamma_\phi \frac{\partial \phi}{\partial x}\right)+\frac{\partial}{\partial y}\left(\Gamma_\phi \frac{\partial \phi}{\partial y}\right)\right] dV + \int_{\delta v} S_\phi \, dV \tag{6}$$

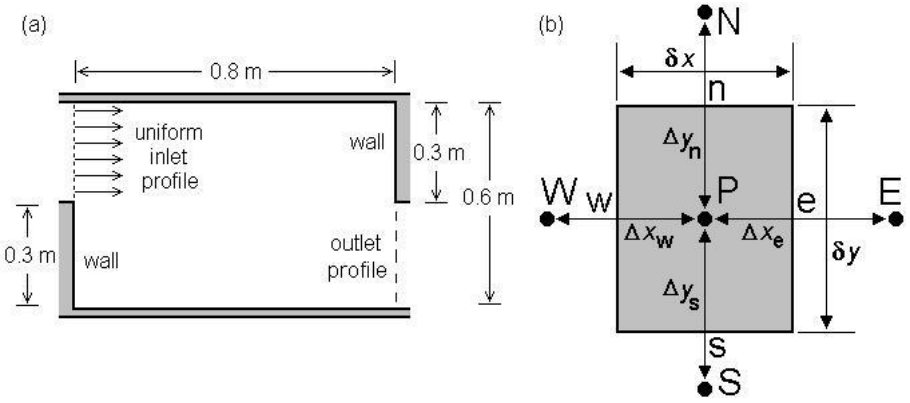

Figure 1. Sketch of (*a*) the laminar flow simulated and (*b*) a typical CV to perform discretization.

Interface values were taken as being those in the middle of the CV interface. For that reason, integration of convective (on the left-hand side of the previous equation) resulted in:

$$C_e \phi_e - C_w \phi_w + C_n \phi_n - C_s \phi_s \tag{7}$$

Convective mass fluxes across the CV interface were evaluated as

$$C_e = (\rho v_x)_e \, \delta y \quad , \quad C_w = (\rho v_x)_w \, \delta y \quad , \quad C_n = (\rho v_y)_n \, \delta x \quad , \quad C_s = (\rho v_y)_s \, \delta x \tag{8}$$

The Flux Blended Deferred Correction (FBDC) scheme was used to perform internodal interpolation for convective terms (KHOSLA e RUBIN, 1974). In such scheme, interface values are approximated as a linear combination of Central Difference Scheme (CDS) and Upwind Difference Scheme (UDS) values:

$$\phi_{face} = \zeta \phi_{face}^{CDS} + (1-\zeta)\phi_{face}^{UDS} = \phi_{face}^{UDS} + \zeta\left(\phi_{face}^{CDS} - \phi_{face}^{UDS}\right)^* \tag{9}$$

where the starred (*) quantities in the last expression come from the previous iteration and ϕ stands for v_x or v_y. The combination factor ζ may vary from 0 (pure UDS) to 1 (pure CDS).

Integration of the diffusive fluxes in Eqs. (4) and (5) having in mind that $\Gamma_\phi = \mu$ resulted in:

$$\left(\mu \frac{\partial \phi}{\partial x}\right)_e \delta y - \left(\mu \frac{\partial \phi}{\partial x}\right)_w \delta y + \left(\mu \frac{\partial \phi}{\partial y}\right)_n \delta x - \left(\mu \frac{\partial \phi}{\partial y}\right)_s \delta x \tag{10}$$

CDS was again used to discretize the gradients in the above equation, namely:

$$\left(\frac{\partial \phi}{\partial x}\right)_e = \frac{\phi_E - \phi_P}{\Delta x_e} \quad , \quad \left(\frac{\partial \phi}{\partial x}\right)_w = \frac{\phi_P - \phi_W}{\Delta x_w} \quad , \quad \left(\frac{\partial \phi}{\partial y}\right)_n = \frac{\phi_N - \phi_P}{\Delta y_n} \quad , \quad \left(\frac{\partial \phi}{\partial y}\right)_s = \frac{\phi_P - \phi_S}{\Delta y_s} \tag{11}$$

Interface pressure values resulting from the integration of source terms in the momentum equations were obtained by linear interpolation or extrapolation of neighboring grid point values.

3.2 Algebraic Equations

Introducing all the discretizations previously described in the integrated GTE, Eq. (6), the following algebraic equation may be obtained after some manipulation:

$$a_P \phi_P = a_W \phi_W + a_E \phi_E + a_S \phi_S + a_N \phi_N + b \tag{12}$$

whose coefficients are given by:

$$\begin{aligned} a_E &= \max\left[-C_e^*, 0\right] + D_e^* \qquad a_W = \max\left[C_w^*, 0\right] + D_w^* \\ a_N &= \max\left[-C_n^*, 0\right] + D_n^* \qquad a_S = \max\left[C_s^*, 0\right] + D_s^* \qquad a_P = a_E + a_W + a_N + a_S \end{aligned} \tag{13}$$

As an illustration, the diffusive flux through the east interface ("*e*" in Fig. 1*b*) is evaluated as:

$$D_e^* = \frac{\mu_e^* \, \delta y}{\Delta x_e} \tag{14}$$

The independent term b receives contributions from source terms (pressure gradients) as well as from the FBDC scheme terms (RABI, 1998).

As the program is running in a preliminary version yet, pressure-velocity coupling is not accomplished by means of a state equation, like Eq. (2), but following the Semi-Implicit Method for Pressure-Linked Equations (SIMPLE) algorithm (PATANKAR e SPALDING, 1972). Mathematically, an algebraic equation for p similar to Eq. (12) is achieved, whose source term is related to the mass imbalance from the continuity equation since approximated velocity fields are provided from the momentum equations.

3.3 Multigrid Method

Locating a CV via indexes i and j for x and y directions respectively, Eq. (12) can be written as:

$$a_P \phi^{ij} - a_W \phi^{i-1j} - a_E \phi^{i+1j} - a_S \phi^{ij-1} - a_S \phi^{ij+1} = b^{ij} \tag{15}$$

Assembling the above equation for each CV in the solution domain results in an system of the form:

$$\mathbf{A}_k \, \mathbf{\Phi}_k = \mathbf{B}_k \tag{16}$$

where $\mathbf{A}_k$ is the coefficient matrix, $\mathbf{\Phi}_k$ is the unknown matrix and $\mathbf{B}_k$ stores all source terms. Index k refers to a given grid level with $k = 1$ corresponding to the coarsest grid and $k = M$ to the finest.

Iterative methods may be used to solve (i.e. relax) Eq. (16). To visualize some flow details, well-refined meshes are needed, which tends to augment the computational effort. In classical methods (Jacobi, Gauss-Seidel, TDMA), convergence rates of the numerical solution are greatest at the beginning of calculations, slowing down sensibly as the iterative process goes on.

A spectral analysis reveals that any smoothing algorithm is capable of reducing efficiently only those Fourier error components whose wavelengths are smaller than or comparable to the mesh spacing (HACKBUSCH, 1985). In order words, after a while only low wavelength error components are indeed reduced and time increase is due to a weak smoothing behavior of large wavelength error components.

To overcome this drawback, the multigrid technique uses a sequence of grids of increasing coarseness instead of iterating at a single grid. In doing so, a broader wavelength spectrum may be covered as long wavelengths in a fine mesh become smaller in a coarse one, where they can then be smoothed.

Hence, in each grid level, the corresponding error components are efficiently reduced, accelerating convergence.

After the equation system has been relaxed by a small number of iterations, an intermediate value $\mathbf{\Phi}'_k$ is obtained along with its correction $\boldsymbol{\phi}_k = \mathbf{\Phi}_k - \mathbf{\Phi}'_k$. Defining the residue as $\mathbf{r}_k = \mathbf{b}_k - \mathbf{A}_k\mathbf{\Phi}'_k$, it is possible to show (HACKBUSCH, 1985) that $\boldsymbol{\phi}_k$ is the solution of the following equation system:

$$\mathbf{A}_k \boldsymbol{\phi}_k = \mathbf{r}_k \tag{17}$$

This previous system can be better approximated as a coarser grid equation:

$$\mathbf{A}_{k-1} \boldsymbol{\phi}_{k-1} = \mathbf{r}_{k-1} \quad , \quad \text{with} \quad \mathbf{r}_{k-1} = I_k^{k-1}\mathbf{r}_k \tag{18}$$

The restriction operator I_k^{k-1} takes values from grid k to grid $k-1$, as sketched in Fig. 2*a*. Once the correction approximation $\boldsymbol{\phi}'_{k-1}$ has been obtained, the prolongation operator I_{k-1}^{k} takes it back to the immediate finer grid, as suggested by Fig. 2*b*, so as to refine the intermediate value $\mathbf{\Phi}'_k$ according to:

$$\mathbf{\Phi}_k^{new} = \mathbf{\Phi}'_k + \boldsymbol{\phi}'_k \quad , \quad \text{with} \quad \boldsymbol{\phi}'_k = I_{k-1}^{k}\boldsymbol{\phi}'_{k-1} \tag{19}$$

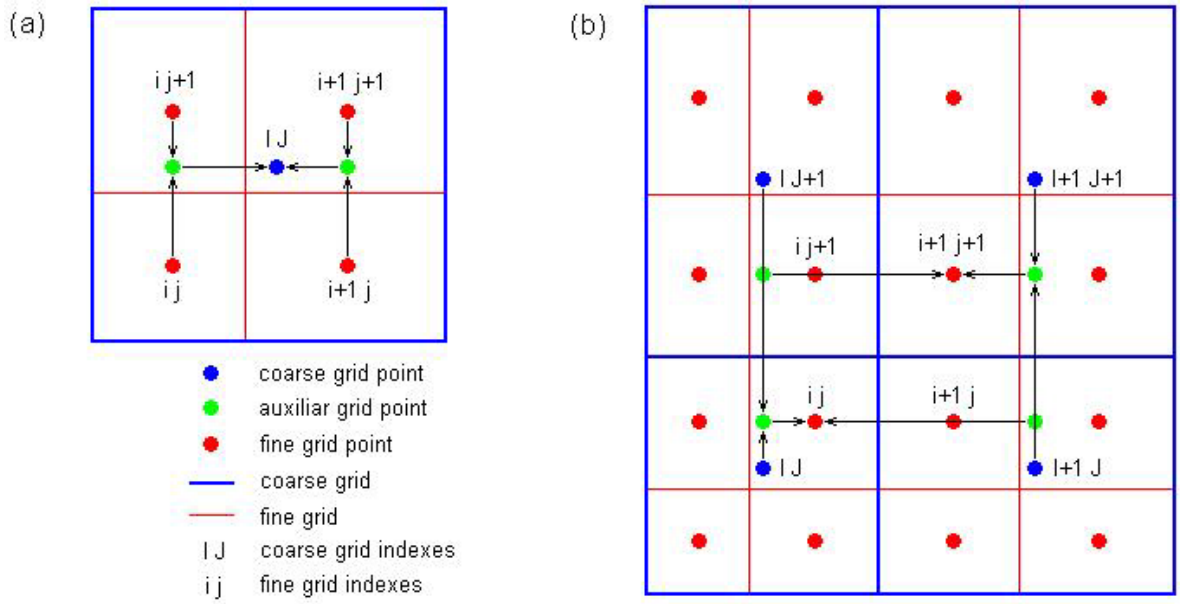

Figure 2. Sketch of (*a*) restriction and (*b*) prolongation operations.

The residue restriction, as suggested in Eq. (18), is accomplished by summing up the residues of the four fine grid CVs that compose the corresponding coarse grid CV. Mathematically:

$$r_{k-1}^{I\,J} = r_k^{i\,j} + r_k^{i\,j+1} + r_k^{i+1\,j} + r_k^{i+1\,j+1} \tag{20}$$

Prolongation is achieved by bilinear interpolation. A temporary intermediate mesh between the coarse and fine grids store values resulting from the application of I_{k-1}^{k} along a single coordinate. Afterwards, the I_{k-1}^{k} operator is applied over those temporary grid points along the remaining orthogonal direction.

Coefficients in matrix $\mathbf{A}_k$ contain diffusive and convective contributions that need special treatment when changing grid level. Diffusive terms are fully recalculated since they depend upon grid

geometry (internodal distances and CV dimensions). Fine grid mass fluxes (convective terms) are summed up at the CV faces in order to compose the corresponding coarse grid mass flux.

The sequence as how all previous operations are concatenated through all existing k-values (i.e. grid levels) distinguishes the so-called V-cycle from the W-cycle. Figure 3 compares these two multigrid cycles for a 4-grid iteration where s = pre-smoothing, r = restriction, cg = coarsest grid iteration and p = prolongation (post-smoothing iterations are not pictured for simplicity).

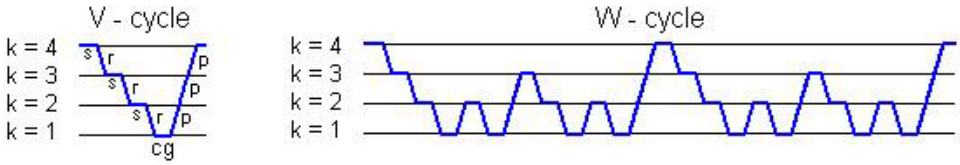

Figure 3. Sequence of operations in a 4-grid iteration: V-cycle and W-cycle.

4. NUMERICAL RESULTS

In order to keep the flow sketched in Fig. 1*a* under laminar regime, a 1.0 kg/m^3 density and 10^{-4} kg/m·s viscosity fluid was adopted, having an inlet velocity of 0.01 m/s. A three-grid method was employed; the finest mesh having NI = 128 CVs along the x-direction and NJ = 96 CVs along the y-direction. Pure UDS ($\zeta = 0$) was employed as interpolation scheme and the number of pre-smoothing, post-smoothing and coarsest grid iteration was fixed at one in a V-cycle strategy.

The numerically obtained flow field can be qualitatively visualized in Fig. 4*a*. The reduction histories of velocity and pressure normalized residues for both the three-grid (3g) and single-grid (1g) solutions are pictured in Fig 4*b*. Such residues are calculated and normalized according to

$$R^2 = \frac{\sum_{ij} r_{ij}^2}{(NI-2)(NJ-2)} \quad , \quad \text{where} \quad r_{ij} = A_P \phi_P - \left(\sum_{nb} A_{nb} \phi_{nb} \right) \tag{21}$$

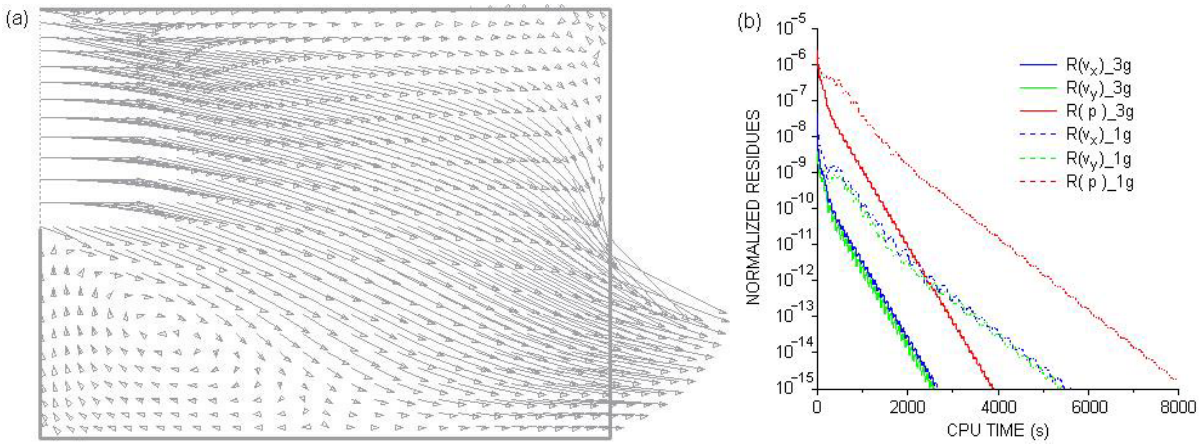

Figure 4. (*a*) Three-grid solution visualization; (*b*) residue reduction histories for v_x, v_y and p.

5. CONCLUSION

Comprehensive modeling of HVAC&R problems may evoke the continuity equation, the Navier-Stokes equations, Fick's law and the first law of thermodynamics. The mathematical complexity may be further extended if turbulence and transient phenomena should be taken into account. For problems like the boundary layer over vertical walls, knowledge of detailed flow behavior is crucial

for the understanding of the whole building thermal performance. In such instances, the analyst may rely on CFD programs.

A V-cycle correction-storage multigrid CFD Fortran-90 program has been initiated and the numerical solution of a two-dimension laminar steady-state internal flow problem was attempted as a first round test. The numerical method also included finite-volume discretization and the SIMPLE pressure-velocity coupling on structured, orthogonal and non-uniform meshes.

As far as computational effort (CPU time spent) is concerned, results showed a better performance (i.e., convergence speed up) of the three-grid solution against the single-grid counterpart without qualitatively jeopardizing the flow field pattern. This is a desired feature if the computational simulator is to be extended to cover HVAC&R problems in a more comprehensive way so as to include turbulence as well as heat and moisture transfers that could in principle slow down the numerical convergence.

Accordingly, short-term new features of the mathematical model and its corresponding CFD simulation program should include a state equation (e.g. ideal gas) and a turbulence model (e.g. mixing length or k-ε) so as to describe properly the internal air flow behavior. Long-term inclusions refer to mass transfer modeling (i.e. moisture considered) and coupling with external thermal phenomena.

6. REFERENCES

BARROS, L.A.F., GRAÇA, V.A.C., KOWALTOWSKI, D.C.C.K., MORAES, O., RUSCHEL, R.C. (2001) Aplicação de simulação computacional no projeto padrão de creche. In: VI ENCONTRO NACIONAL SOBRE CONFORTO NO AMBIENTE CONSTRUÍDO, São Pedro. *Anais*. Grupo de Trabalho em Conforto Ambiental e Eficiência Energética – ANTAC.

CUNHA, E.G., SPANNENBERG, M.G., PICCINI, K.C. (2001) Permeabilidade da edificação a partir das esquadrias internas e sua verificação através do software Ventil. In: VI ENCONTRO NACIONAL SOBRE CONFORTO NO AMBIENTE CONSTRUÍDO, São Pedro. *Anais*. Grupo de Trabalho em Conforto Ambiental e Eficiência Energética – ANTAC.

FERNÁNDEZ, A., EGUÍA, S. (2001) Refrescamiento pasivo en edificios: uso del CFD para diferentes propuestas de ubicación de aberturas. In: VI ENCONTRO NACIONAL SOBRE CONFORTO NO AMBIENTE CONSTRUÍDO, São Pedro. *Anais*. Grupo de Trabalho em Conforto Ambiental e Eficiência Energética – ANTAC.

HACKBUSCH, W. (1985) *Multi-Grid Methods and Applications*, Springer-Verlag, Berlin, 377p.

KHOSLA, P.K., RUBIN, S.G. (1974) A diagonally dominant second-order accurate implicit scheme. *Computational Fluids*, Vol. 2, No. 12, pp. 207, 1974.

LÔBO, D.G.F., BITTENCOURT, L.S. (2001) A influência dos captadores de vento na ventilação natural de habitações populares localizadas em climas quentes e úmidos. In: VI ENCONTRO NACIONAL SOBRE CONFORTO NO AMBIENTE CONSTRUÍDO, São Pedro. *Anais*. Grupo de Trabalho em Conforto Ambiental e Eficiência Energética – ANTAC.

MALISKA, C.R. (1995) *Transferência de Calor e Mecânica dos Fluidos Computacional*, Livros Técnicos e Científicos Editora, Rio de Janeiro, 424p.

MÁXIMO, G.V., BERTE, V.A. (2001) A utilização do software ARQUITROP em projetos de conforto térmico: o caso da sala de acervo do CDHIS-UFU. In: VI ENCONTRO NACIONAL SOBRE CONFORTO NO AMBIENTE CONSTRUÍDO, São Pedro. *Anais*. Grupo de Trabalho em Conforto Ambiental e Eficiência Energética – ANTAC.

MENDES, N., CELINSKI, F. (2001) Análise comparativa entre programas de previsão de transferência de calor e de umidade. In: VI ENCONTRO NACIONAL SOBRE CONFORTO NO AMBIENTE CONSTRUÍDO, São Pedro. *Anais*. Grupo de Trabalho em Conforto Ambiental e Eficiência Energética – ANTAC.

MORAES, O., LABAKI, L.C. (2001) Avaliação do desempenho térmico de uma residência: comparação entre a aplicação do programa de simulação ARQUITROP e do método do C.S.T.B. In: VI ENCONTRO NACIONAL SOBRE CONFORTO NO AMBIENTE CONSTRUÍDO, São Pedro. *Anais*. Grupo de Trabalho em Conforto Ambiental e Eficiência Energética – ANTAC.

PATANKAR, S.V., SPALDING, D.B. (1972) A calculation procedure for heat, mass and momentum transfer in three-dimensional parabolic flows. *Int. J. Heat and Mass Transfer*, Vol. 15, pp. 1787-1806, 1972.

SCHMID, A.L., (2001) Simulação de desempenho térmico em múltiplas zonas: MESTRE, um sistema brasileiro na linguagem Java. In: VI ENCONTRO NACIONAL SOBRE CONFORTO NO AMBIENTE CONSTRUÍDO, São Pedro. *Anais*. Grupo de Trabalho em Conforto Ambiental e Eficiência Energética – ANTAC.

WHITE, F.M. (1991) *Viscous Fluid Flow*, McGraw-Hill Inc., New York, 614p.